

# High Fidelity Singlet-Triplet $S-T_-$ Qubits in Inhomogeneous Magnetic Fields

Clement H. Wong, M. A. Eriksson, S. N. Coppersmith, and Mark Friesen  
*Department of Physics, University of Wisconsin-Madison, Madison, Wisconsin 53706, USA*  
(Dated: September 16, 2022)

We propose an optimal set of quantum gates for a singlet-triplet qubit in a double quantum dot with two electrons utilizing the  $S-T_-$  subspace. Qubit rotations are driven by the applied magnetic field and a field gradient provided by a micromagnet. We optimize the fidelity of this qubit as a function of magnetic fields, taking advantage of “sweet spots” where the rotation frequencies are independent of the energy level detuning, providing protection against charge noise. We simulate gate operations and qubit rotations in the presence of quasistatic noise from charge and nuclear spins as well as leakage to nonqubit states, and predict that in silicon quantum dots gate fidelities greater than 99% can be achieved for two nearly-orthogonal rotation axes.

## I. INTRODUCTION

Electron spins in semiconductor quantum dots are promising qubits because of the long coherence times found in such devices and their potential for scalability.<sup>1</sup> Single-electron spins have been manipulated by applied AC magnetic fields in both III-V and group-IV devices.<sup>2-4</sup> By incorporating micromagnets<sup>5</sup> near the quantum dot, AC electric fields can be used for coherent manipulation of single spins.<sup>6,7</sup> Magnetic field differences can also be generated by pumping of the nuclear spin bath,<sup>8,9</sup> or effective fields can be created by electric-field motion in high spin-orbit materials.<sup>10</sup>

By working with two electrons in a double quantum dot, qubits can be formed from the singlet  $S$  and triplet  $T_0$  states.<sup>9,11-14</sup> A magnetic field difference between the quantum dots enables full control of the  $S-T_0$  subspace by controlling the detuning energy  $\epsilon$  between the dots, with the eigenstates varying from  $\{\downarrow\uparrow, \uparrow\downarrow\}$  to  $\{S, T_0\}$  in different working regimes. Recently, an alternative two-electron qubit has been studied, consisting of the singlet  $S$  and polarized triplet  $T_+$  states for GaAs<sup>15-21</sup> or the  $S$  and  $T_-$  states for Si.<sup>14</sup> Coherent oscillations have been observed in experiment,<sup>18,22</sup> and theory predicts that such oscillations can be high speed.<sup>19</sup> However, it remains unclear whether this qubit can achieve fidelities high enough to meet the threshold for quantum error correction.

In this work, we determine the optimal working points for pulsed-gating manipulation of the  $S-T_-$  (or, equivalently,  $S-T_+$ ) qubit. The points occur in a regime of magnetic fields and field gradients that has not been explored previously. The required field gradients are easily achieved with micromagnets. Using realistic assumptions about experimental noise derived from recent experiments, we demonstrate that control fidelities in excess of 99% can be realized in natural abundance Si. The calculated fidelities are high enough to achieve fault-tolerant operation using surface code error correction.<sup>23</sup> Interestingly, only one of the optimal operating points is at a charge-noise sweet spot. The other optimal point is detuned from the second charge-noise sweet spot, in order to avoid leakage driven by the magnetic field dif-

ference between the quantum dots. Using realistic parameters, we find gate speeds of 43 MHz for  $X$ -rotations and 124 MHz for  $Z$ -rotations. These gate speeds can be increased by simultaneously increasing applied magnetic fields and the tunnel coupling.

This paper is organized as follows. In section II, we review the two-electron double dot Hamiltonian including all relevant states. In section III, we describe the magnetic field configuration required to implement the  $S-T_-$  qubit, discuss single and two-qubit gates, and deduce the optimal parameter regime based on qualitative arguments. In section IV, we present the method we use to simulate qubit gates in the presence of environmental noise and present our results for  $X$  and  $Z$  gate fidelities. Supporting materials are given in the appendices, including results for gate fidelities when the tunnel coupling has an exponential dependence on detuning, a review of the qubit effective Hamiltonian, discussion of leakage oscillations, results for the process matrix at the optimal working point, and a derivation of dephasing rates with and without nuclear noise.

## II. DOUBLE DOT HAMILTONIAN

In this section, we review the Hamiltonian for two-electron states in a double quantum dot. We start with a Hubbard Hamiltonian,<sup>15,17</sup>

$$H = \frac{t_c}{\sqrt{2}}(\vec{c}_L^\dagger \vec{c}_R + \vec{c}_R^\dagger \vec{c}_L) + H_Z(\mathbf{B}_i, \mathbf{h}_i) - \sum_{i=L,R} \mu_i(n_{i\uparrow} + n_{i\downarrow}) + U n_{i\uparrow} n_{i\downarrow}$$

where  $\vec{c}_i$  is the two-component spinor annihilation operator for electrons at the dot  $i$ ,  $L$  and  $R$  denotes left and right dots,  $n_{i\sigma} = c_{i\sigma}^\dagger c_{i\sigma}$  is the spin  $\sigma$  electron number operator,  $t_c/\sqrt{2}$  is the tunnel coupling between the dots,  $\mu_i$  are electrochemical potentials,  $\uparrow$  and  $\downarrow$  denote spin up and down along a spin quantization axis, and  $U$  is the intradot Coulomb interaction energy.<sup>24</sup> The detuning is defined by  $\epsilon = \mu_L - \mu_R - U$ , so that  $\epsilon=0$  corresponds to the  $(1, 1) \rightarrow (0, 2)$  charge transition. We consider local static magnetic fields and fluctuating nuclear

Overhauser fields are denoted by  $\mathbf{B}_i$  and  $\mathbf{h}_i$ , respectively. The Zeeman Hamiltonian  $H_Z$  is given by  $H_Z(\mathbf{B}_i, \mathbf{h}_i) = g\mu_B \sum_{i=L,R} (\mathbf{B}_i + \mathbf{h}_i) \cdot \mathbf{S}_i$ , where  $\mathbf{S}_i = \vec{c}_i^\dagger \boldsymbol{\sigma} \vec{c}_i / 2$  are the spin density operators on the left and right dots,  $\boldsymbol{\sigma}$  are the Pauli matrices,  $g \simeq 2$  is the effective Landé electron  $g$ -factor in silicon,  $\mu_B$  is the Bohr magneton.

In the parameter regime of our proposed qubit, the tunnel coupling is the largest energy scale, so that a hybridized  $\{(1, 1), (0, 2)\}$  charge basis is appropriate.<sup>25</sup> Only tunneling between singlets  $S(0, 2)$  and  $S(1, 1)$  are relevant because spin flipping transitions between singlets and triplets are negligible, as spin-orbit coupling is very weak in silicon.<sup>26</sup> The Hamiltonian in the singlet subspace of  $\{(1, 1), (0, 2)\}$  charge states is thus given by

$$H_S = t_c(|S(1, 1)\rangle\langle S(0, 2)| + \text{h.c.}) - \epsilon|S(0, 2)\rangle\langle S(0, 2)|.$$

The eigenstates are hybridized charge states given by

$$\begin{pmatrix} |S\rangle \\ |S'\rangle \end{pmatrix} = \begin{pmatrix} \cos \eta & \sin \eta \\ -\sin \eta & \cos \eta \end{pmatrix} \begin{pmatrix} |S(1, 1)\rangle \\ |S(0, 2)\rangle \end{pmatrix}, \quad (1)$$

with eigenvalues

$$\begin{pmatrix} E_S \\ E_{S'} \end{pmatrix} = t_c \begin{pmatrix} \tan \eta \\ -\cot \eta \end{pmatrix} = \frac{1}{2} \begin{pmatrix} -\epsilon - \sqrt{4t_c^2 + \epsilon^2} \\ -\epsilon + \sqrt{4t_c^2 + \epsilon^2} \end{pmatrix},$$

where we have parametrized the admixture of charge states by the mixing angle  $\eta$ , with  $\cos \eta$  and  $\sin \eta$  being the amplitudes of the projections of  $|S\rangle$  onto the  $(1, 1)$

and  $(0, 2)$  charge states, respectively. See the inset of Fig. 3 for a plot of their magnitudes as a function of detuning. The lower singlet state  $|S\rangle$  approaches  $|S(1, 1)\rangle$  when  $\epsilon \ll 0$ , and it approaches  $|S(0, 2)\rangle$  when  $\epsilon \gg 0$ , while the excited singlet state  $|S'\rangle$  has the opposite asymptotic behavior.

To evaluate the Hamiltonian in the singlet and triplet basis of spin states, defined by

$$\begin{aligned} |S\rangle &= \frac{|\uparrow\downarrow\rangle - |\downarrow\uparrow\rangle}{\sqrt{2}}, & |T_0\rangle &= \frac{|\uparrow\downarrow\rangle + |\downarrow\uparrow\rangle}{\sqrt{2}}, \\ |T_+\rangle &= |\uparrow\uparrow\rangle, & |T_-\rangle &= |\downarrow\downarrow\rangle, \end{aligned}$$

it is useful to express the Zeeman Hamiltonian in terms of the total spin  $\mathbf{S}_L + \mathbf{S}_R$  and spin difference  $\mathbf{S}_L - \mathbf{S}_R$  on the two dots. For the static fields, it is given by

$$H_Z(\mathbf{B}_i) = g\mu_B [\mathbf{B}_{\text{avg}} \cdot (\mathbf{S}_L + \mathbf{S}_R) + \frac{\Delta\mathbf{B}}{2} \cdot (\mathbf{S}_L - \mathbf{S}_R)],$$

where we define the average field  $\mathbf{B}_{\text{avg}} = (\mathbf{B}_L + \mathbf{B}_R)/2$  and the difference field  $\Delta\mathbf{B} = \mathbf{B}_L - \mathbf{B}_R$ . The Zeeman Hamiltonian of the nuclear fields  $H_Z(\mathbf{h}_i)$  is analogously expressed in terms of the average nuclear field  $\mathbf{h} = (\mathbf{h}_L + \mathbf{h}_R)/2$  and nuclear field difference  $\Delta\mathbf{h} = \mathbf{h}_L - \mathbf{h}_R$ .

Defining the quantization axis ( $\hat{\mathbf{z}}$ ) along the constant average field direction  $\mathbf{B}_{\text{avg}} = B_z \hat{\mathbf{z}}$ , the Hamiltonian projected onto the subspace spanned by the basis  $\{|T_+(1, 1), T_0(1, 1), T_-(1, 1), S, S'\rangle$  is given by<sup>15,27</sup>

$$H = g\mu_B \begin{pmatrix} B_z + h_z & h_+/2 & 0 & \cos \eta \frac{\Delta B_+ + \Delta h_+}{2\sqrt{2}} & -\sin \eta \frac{\Delta B_+ + \Delta h_+}{2\sqrt{2}} \\ h_-/2 & 0 & h_+/2 & \cos \eta \frac{\Delta B_z + \Delta h_z}{2} & -\sin \eta \frac{\Delta B_z + \Delta h_z}{2} \\ 0 & h_-/2 & -B_z - h_z & -\cos \eta \frac{\Delta B_- + \Delta h_-}{2\sqrt{2}} & \sin \eta \frac{\Delta B_- + \Delta h_-}{2\sqrt{2}} \\ \cos \eta \frac{\Delta B_- + \Delta h_-}{2\sqrt{2}} & \cos \eta \frac{\Delta B_z + \Delta h_z}{2} & -\cos \eta \frac{\Delta B_+ + \Delta h_+}{2\sqrt{2}} & -J/g\mu_B & 0 \\ -\sin \eta \frac{\Delta B_- + \Delta h_-}{2\sqrt{2}} & -\sin \eta \frac{\Delta B_z + \Delta h_z}{2} & \sin \eta \frac{\Delta B_+ + \Delta h_+}{2\sqrt{2}} & 0 & E_{S'}/g\mu_B \end{pmatrix}, \quad (2)$$

where  $h_\pm = h_x \pm ih_y$ ,  $\Delta B_\pm = \Delta B_x \pm i\Delta B_y$ , and the exchange energy  $J$  is given by  $J = -E_S = (\epsilon/2) + \sqrt{(\epsilon/2)^2 + t_c^2}$ . The factors  $\cos \eta$  and  $\sin \eta$  appear in the couplings between singlet and triplets because the magnetic field differences that mix these spin states only couple to the  $(1, 1)$  charge state.

Gate operations for the  $S$ - $T_-$  qubit we propose occur deep in the  $(1, 1)$  charge regime where  $J/t_c \ll 1$  and  $(\cos \eta, \sin \eta) \simeq (1, -J/t_c)$  as shown in the inset of Fig. 3. In this regime, the high energy singlet  $|S'\rangle$  can be neglected because the leakage probability from the triplets to  $S'$  is proportional to  $\sin^2 \eta^2 (|\Delta\mathbf{B}|/E_{S'})^2 \approx J^4 \Delta\mathbf{B}^2 / t_c^6 \approx 0$ , as confirmed in our numerical simulations described in appendix C. Therefore, for the operating regime of interest ( $J \ll t_c$ ), the physically relevant Hamiltonian is effectively reduced to the upper  $4 \times 4$  block of Eq. (2). The Rabi flopping terms due to the average fields  $h_\pm$  can

also be neglected because they lead to effects of order  $(h_\pm/B_z)^2 \simeq 10^{-6}$  in the parameter regime we consider.

### III. DC PULSED-GATED $S$ - $T_-$ QUBIT

In this work, we consider a DC pulsed-gated  $S$ - $T_-$  qubit in an applied magnetic field gradient provided by a micromagnet, as illustrated in Fig. 1. A typical double dot geometry incorporating a micromagnet is shown in Fig. 1(a). There are three contributions to the total field: the uniform external field  $\mathbf{B}^{\text{ext}}$ , whose magnitude and direction are assumed to be tunable, the field from a micromagnet  $\mathbf{B}^{\text{m}}$ ,<sup>5,14</sup> and the slowly varying Overhauser fields arising from the nuclear spins.<sup>29</sup> The energy levels of the two-electron double dot [Eq. (2)] as a function of the detuning  $\epsilon$ , are sketched in Fig. 1(c).

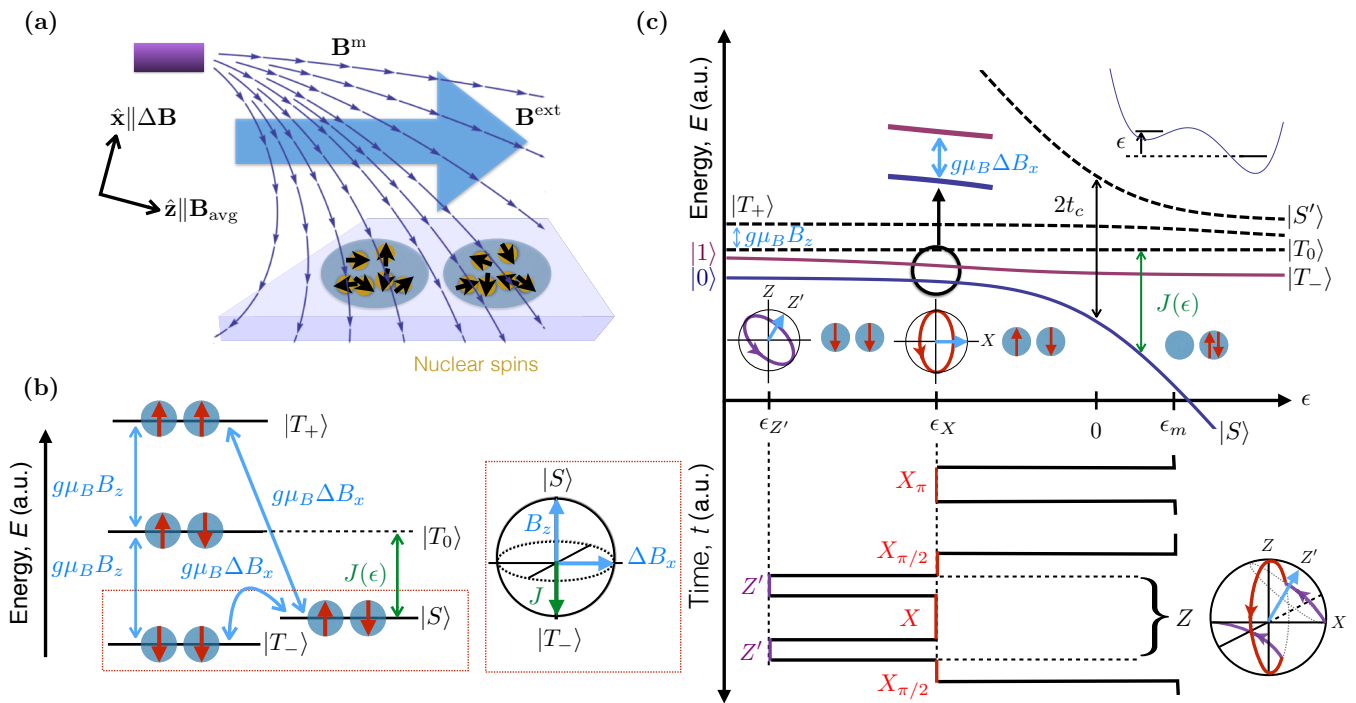


FIG. 1. (color online). (a) Illustration of a nonuniform magnetic field  $\mathbf{B}^m$  provided by a micromagnet (purple rectangle) fabricated above a double quantum dot, and a uniform external field  $\mathbf{B}^{\text{ext}}$  (blue arrow). Random, quasistatic Overhauser fields are also present, due to nuclear spins. (b) Singlet-triplet energy diagram, showing the dominant couplings between levels (arrows). A Bloch sphere representation of the  $S$ - $T_-$  qubit indicates the rotation axes associated with the different coupling terms. (c) Top: singlet-triplet energy diagram as a function of detuning  $\epsilon$ .  $X$ -rotations are performed at a detuning sweet spot (black circle at  $\epsilon_X$ ) where the qubit energy levels are parallel and the splitting is set by  $\Delta B_x$ .  $Z'$ -rotations occur in the far-detuned regime ( $\epsilon_{Z'}$ ), with a rotation axis  $Z'$  tilted slightly away from  $Z$  on the Bloch sphere. Bottom: illustration of typical pulse sequences for implementing  $X$  and  $Z$ -rotations. Measurement of the singlet probability is done at the detuning  $\epsilon_m > 0$  in the  $(0, 2)$  charge state. The  $Z$  protocol shows a Ramsey pulse sequence where the  $Z$ -rotation is implemented using a three-step sequence<sup>28</sup> to correct for the tilt of the  $Z'$  axis, as illustrated on the Bloch sphere.

Figure 1(b) shows the singlet-triplet energy splittings near the  $S$ - $T_-$  crossing, with transitions due to the static field difference  $\Delta \mathbf{B}$  indicated. The logical  $S$ - $T_-$  qubit consists of the subspace of the  $S$  and  $T_-$  states.  $S$ - $T_0$  oscillations, driven by  $\Delta B_z$ , correspond to leakage outside the qubit subspace. For a given  $\Delta \mathbf{B}$ , we eliminate this process by arranging  $\mathbf{B}^{\text{ext}}$  such that  $\Delta B_z = \Delta \mathbf{B} \cdot \mathbf{B}_{\text{avg}} = 0$ . This condition is satisfied when

$$\cos \theta_0 = \frac{\mathbf{B}_R^{m2} - \mathbf{B}_L^{m2}}{2|\Delta \mathbf{B}||\mathbf{B}^{\text{ext}}|}, \quad (3)$$

where  $\theta_0$  is the relative angle between the externally applied field and the difference field defined by  $\cos \theta_0 = \mathbf{B}^{\text{ext}} \cdot \Delta \mathbf{B} / |\mathbf{B}^{\text{ext}}||\Delta \mathbf{B}|$ . In deriving Eq. (3) we used the fact that the static field difference comes only from the micromagnet field, so that  $\Delta \mathbf{B} \simeq \mathbf{B}_L^m - \mathbf{B}_R^m$ .

Eq. (3) shows that  $\Delta B_z$  can be eliminated, provided that one can control the direction of  $\mathbf{B}^{\text{ext}}$ , while its magnitude  $|\mathbf{B}^{\text{ext}}|$  can still be freely adjusted to optimize the qubit as a function of the average field  $B_z$ . Experimentally, directional control of the external field can be implemented, for example, by using a vector magnet. Since

we will find that only small magnetic fields (mT) are sufficient for a high fidelity  $S$ - $T_-$  qubit, directional control of  $\mathbf{B}^{\text{ext}}$  can also be achieved with magnetic fields sourced by current carrying wires. At the optimal working point given in section IV, our qubit can tolerate a magnetic field misalignment as large as  $\Delta B_z / \Delta B_x = 10\%$ , which yields leakage less than 0.1% (See appendix C).

After arranging  $\Delta B_z \simeq 0$ , we define the  $x$ -axis such that  $\Delta \mathbf{B} = \Delta B_x \hat{\mathbf{x}}$ , which mainly drives  $S$ - $T_-$  oscillations. Representing the qubit on a Bloch sphere with  $|S\rangle = |Z\rangle$  ( $|T_- \rangle = |-Z\rangle$ ) on the north (south) poles, the action of  $\Delta B_x$  corresponds to an  $X$ -rotation on the Bloch sphere, while  $B_z$  and the exchange interaction  $J$  combine to produce  $Z$ -rotations, as illustrated in Fig. 1(b).

While the results reported in this work use the full 5D Hamiltonian (2) that includes the states  $S$ ,  $T_-$ ,  $T_0$ ,  $T_+$ , and  $S'$  to properly account for leakage in the time evolution, it is instructive to consider the Hamiltonian

projected onto the  $S-T_-$  subspace,<sup>27</sup>

$$H^{(ST_-)} = -g\mu_B \quad (4)$$

$$\left( \begin{array}{cc} J(\epsilon)/g\mu_B & \frac{\cos\eta(\epsilon)}{2\sqrt{2}}(\Delta B_x + \Delta h_+) \\ \frac{\cos\eta(\epsilon)}{2\sqrt{2}}(\Delta B_x + \Delta h_-) & B_z + h_z \end{array} \right).$$

This Hamiltonian is the leading term in the effective Hamiltonian obtained by a canonical transformation.<sup>15</sup> Higher order terms, derived in Appendix B, are negligibly small in the parameter regime of interest. Thus, the Hamiltonian (4) contains all qubit dynamics except for leakage effects. We note that, in contrast to the  $S-T_-$  qubit proposed in this work, Ref. [15] proposes utilizing the *single* spin states on one dot (R) as the logical qubit states, which requires the parameter regime  $B_R^z \ll t_c \ll B_L^z \simeq B_z$ , different than the  $S-T_-$  qubit given in Eq. (5) below.

The Hamiltonian (4) enables complete electrical control of the logical qubit through the relative energy detuning  $\epsilon$  between the (0, 2) and (1, 1) charge states, as indicated in Fig. 1(c).  $X$ -rotations are performed at the detuning  $\epsilon_X$  defined by  $J(\epsilon_X) = g\mu_B B_z$ , where the  $S-T_-$  energy levels anticross, and rotations about an axis close to  $Z$ , denoted by  $Z'$ , is performed at a large negative detuning, labeled  $\epsilon_{Z'}$ , where  $g\mu_B B_z \gg J$ . Initialization into  $|S\rangle$  can be performed deep in the (0, 2) charge regime ( $\epsilon \gg 0$ ), where singlet-triplet couplings vanish ( $\cos\eta \rightarrow 0$ ).

The main challenge in achieving a high fidelity  $S-T_-$  qubit are  $X$ -rotations, which are susceptible to dephasing due to detuning noise that cause fluctuations in the energy gap  $E_{01}$  between the energy levels  $|0\rangle$  and  $|1\rangle$  of Eq. (4). Although the anticrossing point  $\epsilon_X$  is a detuning sweet spot where  $\partial E_{01}/\partial\epsilon = 0$ ,  $E_{01}$  being the energy gap between the qubit energy levels  $|0\rangle$  and  $|1\rangle$ , higher order fluctuations  $\sim \partial^2 E_{01}/\partial\epsilon^2$  can be important due to the large detuning noise. Increasing  $\Delta B_x$  alone to combat detuning noise is problematic as it would require very large fields,  $g\mu_B B_x \gg \sigma_\epsilon = 5 \mu\text{eV}$ , and increase leakage to  $T_+$ , which scales as  $(\Delta B_x/B_z)^2$ . These considerations suggests that the optimal regime for the  $S-T_-$  qubit is given by

$$\sigma_h \ll g\mu_B \Delta B_x \ll g\mu_B B_z \ll t_c \quad (5)$$

where  $\sigma_h$  is the nuclear noise variance. The first inequality insures that the  $X$ -gate speeds are much faster than the dephasing rate due to nuclear noise. The second inequality is necessary to suppress leakage from  $S$  to  $T_+$ . The last inequality insures a wide sweet spot at the anticrossing  $\epsilon_X$ , by making the crossing point  $\epsilon_X \simeq -t_c^2/g\mu_B B_z$  occur in the far detuned regime, where  $\sim \partial^2 E_{01}/\partial\epsilon^2 \propto (\partial J/\partial\epsilon)^2 \ll 1$ . In the rest of this paper, we show that within the parameter constraints imposed by Eq. (5), a high fidelity  $S-T_-$  qubit with experimentally feasible parameters can be achieved in silicon. As a comparison with the  $S-T_0$  qubit, we show in appendix E 2 that for parameters such that the rotation frequencies of the  $S-T_0$  and  $S-T_-$  qubits are equal, dephasing rate of

the exchange-driven oscillations in  $S-T_0$  qubit (which is also limited by exchange noise) is twice as fast as the  $X$ -rotations in  $S-T_-$  qubit.

While this work focuses on single qubit gates, we note that capacitive two-qubit gates can be implemented similarly as in the  $S-T_0$  qubit,<sup>30,31</sup> since the capacitive coupling is based only on the Coulomb energy difference between the singlet and triplet orbital states, which do not depend on the particular polarization of the triplets. As an example, for two qubits labeled by  $A$  and  $B$ , the two-qubit interaction due to the dipole-dipole interaction of the  $S(0, 2)$  states is given by

$$H_{AB} = J_{AB}|S\rangle\langle S|_A \otimes |S\rangle\langle S|_B \quad (6)$$

where  $J_{AB} = \Delta E_c(\partial J/\partial\epsilon_A)(\partial J/\partial\epsilon_B)$ ,  $\Delta E_c$  is the difference in the Coulomb energy between  $|(0, 2)\rangle \otimes |(0, 2)\rangle$  and  $|(1, 1)\rangle \otimes |(1, 1)\rangle$  charge states, and  $\partial J/\partial\epsilon_{A,B} = \sin^2\eta(\epsilon_{A,B})$  is proportional to the dipole moments in the  $S(0, 2)$  state of each qubit. The interaction can thus be turned on by pulsing each to the (0, 2) regime at large positive detuning. The coupling in Eq. (6) enables a controlled-phase gate which has recently been experimentally demonstrated in an  $S-T_0$  qubit.<sup>31</sup>

#### IV. GATE FIDELITIES

To aid in designing real physical devices, we perform simulations of qubit rotations to establish the optimal values for the applied magnetic fields and the tunnel coupling. Simulations are performed by numerically integrating the time-dependent Schrödinger equation

$$i\hbar \frac{dc_n}{dt} = \sum_{m=1}^5 H_{nm}(\xi_\alpha) c_m,$$

where  $c_n$  are the expansion coefficients of the wave function in the  $\{T_+(1, 1), T_0(1, 1), T_-(1, 1), S, S'\}$  basis,  $H_{nm}$  are the matrix elements given in Eq. (2), and  $\xi_\alpha$  are noise variables.

The main noise sources in a double dot are typically assumed to be charge fluctuations<sup>32,33</sup> and low-frequency nuclear field fluctuations,<sup>27,34</sup> both of which can be treated as quasistatic on the time scale of the qubit dynamics,<sup>27</sup> and Gaussian distributed with detuning and nuclear noise variances  $\sigma_\epsilon = 5 \mu\text{eV}$ <sup>13,14,35</sup> and  $\sigma_h = 3 \text{neV}$ ,<sup>13,14,29</sup> respectively, as appropriate for natural Si. We account for these quasistatic noise by performing many time evolutions with different values of the noise terms  $\xi_\alpha = (\delta\epsilon, h_z, \Delta h_{x,y,z})$ , where  $\delta\epsilon$  is the deviation from  $\epsilon_X$  or  $\epsilon_{Z'}$  due to detuning noise, and then computing the density matrix with the discretized Gaussian average

$$\rho_{nm} = \prod_{\alpha} \sum_{k_\alpha=-4}^4 \Delta\xi_\alpha [p(\xi_\alpha)(c_n c_m^*)] |_{\xi_\alpha = k_\alpha \sigma_\alpha}, \quad (7)$$

where  $p(\xi_\alpha) = \exp(-\xi_\alpha^2/2\sigma_\alpha^2)/\sqrt{2\pi}\sigma_\alpha$  are Gaussian distributions for  $\xi_\alpha = (\epsilon, h_z, \Delta h_{x,y,z})$  with variances

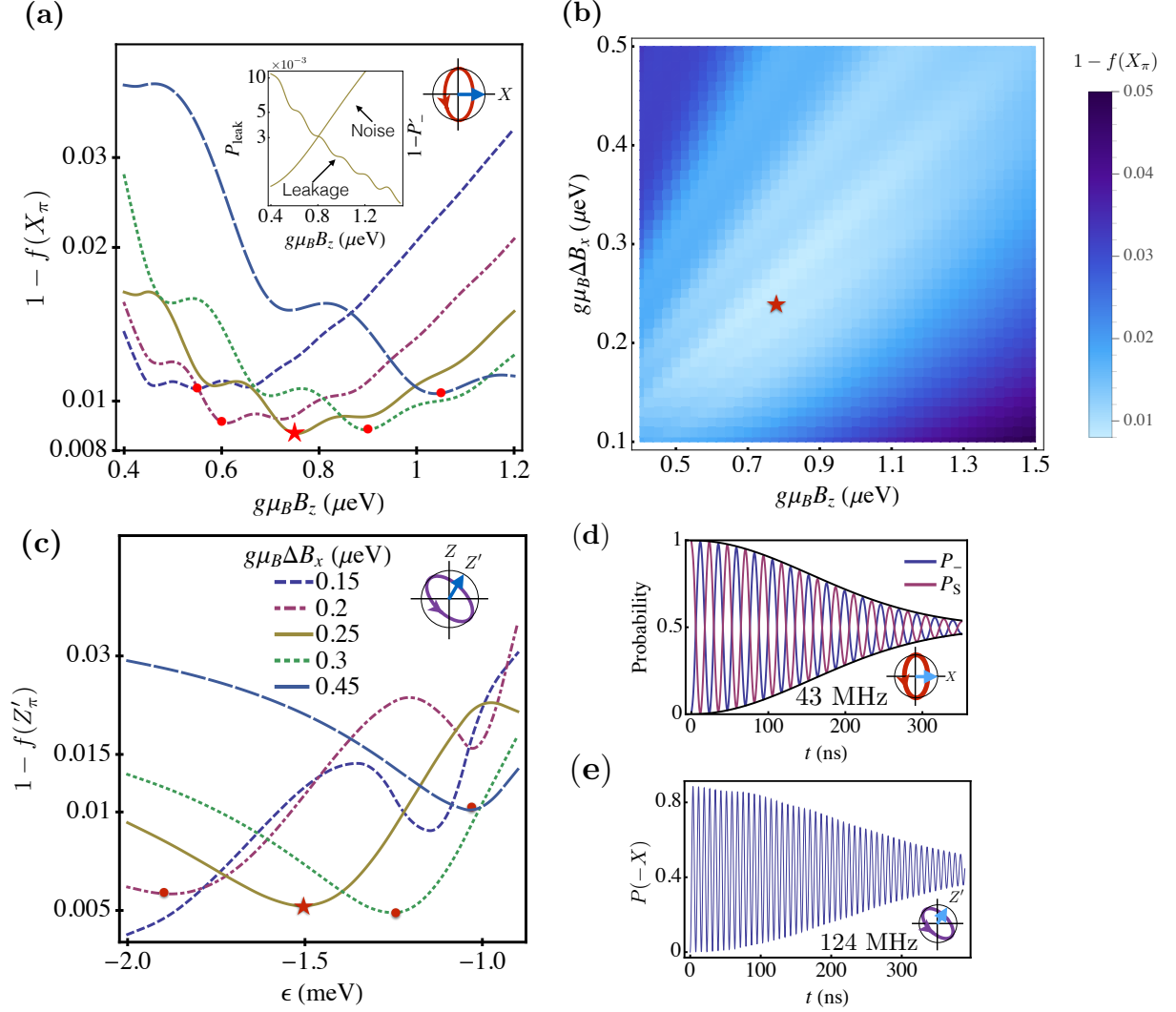


FIG. 2. (color online). (a) Semilog plot of the state infidelity of an  $X_\pi$  rotation,  $1 - f(X_\pi)$ , as a function of the applied longitudinal field  $B_z$ , for several values of the field gradient  $\Delta B_x$ . Inset: a similar plot showing the contributions to the state infidelity due to leakage  $P_{\text{leak}}$ , and the combined effect of charge and nuclear noise  $1 - P_-^l$ , for the case  $g\mu_B\Delta B_x = 0.25 \mu\text{eV}$ ; see Eq. (9). (b) A color density plot of  $1 - f(X_\pi)$  for an  $X_\pi$  rotation, as a function of  $B_z$  and  $\Delta B_x$ . The red star indicates the optimal working point  $g\mu_B(\Delta B_x, B_z) = (0.25, 0.75) \mu\text{eV}$ . (c) Infidelity of  $Z'(\pi)$  rotations as a function of detuning, for nearly-optimal values of  $g\mu_B\Delta B_x$  and  $g\mu_B B_z$  (indicated by the red dots and star in (a)). (d) Larmor oscillations ( $X$ -rotations), and the corresponding Gaussian decay envelope, obtained at the optimal point. (e)  $Z'$ -rotations performed at the starred point in (b), for  $\epsilon_{Z'} = -1.5 \text{ meV}$ .

$\sigma_\alpha = (\sigma_\epsilon, \sigma_h, \sqrt{2}\sigma_h)$ , as appropriate for uncorrelated noise between the left and right dots. The average is discretized over the interval  $\xi_\alpha \in [-4\sigma_\alpha, 4\sigma_\alpha]$  with a step size  $\Delta\xi_\alpha = \sigma_\alpha$ .

To find the optimal points, we optimize a chosen *state* fidelity representative of the  $X$  and  $Z$  gates, and then compute the *process* fidelity for each gate at the optimal point. The process fidelities are defined by  $F(\mathcal{E}) = \text{Tr}[\chi(\mathcal{E})\chi(\mathcal{E}_0)]$ , where  $\mathcal{E}$  and  $\mathcal{E}_0$  denote gate operations with and without noise, respectively, and  $\chi$  is the pro-

cess matrix defined by<sup>36</sup>

$$\mathcal{E}(\hat{\rho}) = \sum_{mn} \hat{E}_m \hat{\rho} \hat{E}_n^\dagger \chi_{mn} \quad (8)$$

where we choose a basis set given by  $\hat{E}_m = \{1, \tau_X, -i\tau_Y, \tau_Z\}$ , and  $\tau_i$  are the Pauli matrices. An explicit formula for the one qubit  $\chi$  matrix is given in appendix D, and the  $\chi$  matrix elements for the two gates considered in section IV are plotted in Fig. 5.

In our simulations, we consider two types of tunnel couplings (i) a constant tunnel coupling, with  $t_c = 20 \mu\text{eV}$ , and (ii) a detuning-dependent coupling,<sup>32</sup> with the exponential dependence  $t_c = t_0 \exp(\epsilon/\epsilon_0)$ , with  $t_0 = 20 \mu\text{eV}$

and  $\epsilon_0=1$  meV chosen to match experimental data for Si.<sup>13</sup> The simulation results shown in Fig. 2 correspond to case (i), while results for case (ii) are reported in Appendix A and Table I. Similar results are obtained in both cases, but depend on the specific parameters used. We note that a tunnel coupling  $t_0=20$   $\mu$ eV is well within the range feasible in experiments, e.g.,  $t_c = 60$   $\mu$ eV has been achieved.<sup>22</sup>

### A. $X$ rotations

We first investigate the fidelity of pulsed  $X_\pi$  rotations, using the pulse sequence shown in the lower portion of Fig. 1(c). The qubit is initialized to state  $|S(0,2)\rangle$  at the detuning value  $\epsilon=\epsilon_m$ . The qubit is then pulsed via ‘‘rapid adiabatic passage’’ (RAP)<sup>11</sup> (fast compared to the  $S$ - $T_-$  rotation frequency but slow compared to the tunneling frequency  $t_c$ ) to the state  $|S\rangle$  at the level anticrossing  $\epsilon_X$ , defined by  $J(\epsilon_X)=g\mu_B B_z$ . For the parameter values at which the gate fidelity is optimized, the RAP ramp from  $(0,2)$  to  $(1,1)$  can be performed so that its contribution to the infidelity due to leakage is negligible ( $<0.1\%$ ). We then evolve the system at  $\epsilon=\epsilon_X$ , perform averages over the quasistatic charge and nuclear noise distributions, and compute the average probabilities  $P_S$ ,  $P_{S'}$ ,  $P_\pm$ , and  $P_0$  of being in the states  $|S\rangle$ ,  $|S'\rangle$ ,  $|T_\pm\rangle$ , and  $|T_0\rangle$ . We consider the state fidelity  $f(X_\pi)=P_-(\tau_X)$ , defined by the probability of reaching the target final state  $|T_-\rangle$  at the  $X_\pi$ -gate period  $\tau_X = \sqrt{2}h/g\mu_B \Delta B_x$ . The corresponding infidelity is given by  $1 - f(X_\pi)$ .

Figure 2 shows the results of our simulations as a function of the magnetic fields  $B_z$  and  $\Delta B_x$ . Figures 2(a) and (b) show that  $X$ -rotation fidelities of 99% should be attainable for the  $S$ - $T_-$  qubit, far higher than in recent experiments<sup>14,21</sup> or theoretical proposals.<sup>37</sup> Long-lived Rabi oscillations are shown in the inset of Fig. 2(d). For case (i), we identify the optimal working point, marked by a star in Fig. 2(b), as  $g\mu_B \Delta B_x=0.25$   $\mu$ eV ( $\Delta B_x=1.5$  mT) and  $g\mu_B B_z=0.75$   $\mu$ eV ( $B_z=4.5$  mT), corresponding to a gate speed of 43 MHz. At this working point, we find the process fidelity  $F(X_\pi) = 99.3\%$ , which is slightly higher than  $f(X_\pi)$ . For comparison, we considered a smaller tunnel coupling,  $t_c=10$   $\mu$ eV, for which we obtain an optimal process fidelity of  $F(X_\pi) = 98.4\%$  at  $g\mu_B(\Delta B_x, B_z)=(0.15, 0.3)$   $\mu$ eV.

The optimal field difference is slightly larger than typical Overhauser fields in GaAs dots<sup>29</sup> ( $\sim 0.1$   $\mu$ eV), and much larger than Overhauser fields in Si dots<sup>29</sup> ( $\sim 3$  neV). Experimentally, gradient fields ( $\Delta B_x$ ) as large as 30 mT (3.5  $\mu$ eV) has been achieved using micromagnets,<sup>5</sup> so that an order of magnitude increase in the  $X$ -gate speed is possible.

In Fig. 2(a), we see that the infidelity goes through a minimum as a function of  $B_z$  for a given  $\Delta B_x$ . This minimum is a result of the competition between leakage and noise. The decreasing  $B_z$  dependence to the left of the minimum indicates that leakage dominates

the infidelity there. This is confirmed in the inset of Fig. 2(a), where we plot total leakage probability (left axis)  $P_{\text{leak}}=P_+ + P_0 + P_{S'}$ , which matches the infidelity to the left of the minimum. The small oscillations in Fig. 2 also arise from coherent leakage oscillations to  $T_+$  caused by  $\Delta B_x$ , resulting in local minima in the infidelity that occurs when the gate period is commensurate with the leakage period.<sup>38</sup> See Fig. 4 for a plot of leakage oscillations to  $T_+$ . The apparent lines of nearly constant infidelity in Fig. 2 (b) correspond to lines of constant leakage that occur at fix ratios of  $\Delta B_x/B_z$ .

Next, we show that the increasing  $B_z$  dependence to the right of the minimum comes from exchange noise  $\delta J = \delta\epsilon(\partial J/\partial\epsilon)$ . To this end, we employ an approximate analytic solution for the qubit dynamics using only the 2D Hamiltonian Eq. (4), averaged over quasistatic noise within the 2D subspace. This solution is derived in Ref. [34] and reviewed in appendix E4, and leads to the final state ( $T_-$ ) probability for the  $X_\pi$  gate (for optimal parameters)

$$P'_-(\tau_X) = \frac{1}{2} \left( 1 + e^{-(\tau_X/T_2^*(X))^2} (1 - \sigma_\perp^2/b^2) \right), \quad (9)$$

where  $\sqrt{2}h/T_2^*(X) = \sigma_h$ ,  $\sigma_\perp^2 = \sigma_J^2 + \sigma_h^2$ ,  $b = g\mu_B |\Delta B_x|/\sqrt{2}$ ,  $\tau_X=h/b$  is the gate time, and  $\sigma_J = \sigma_\epsilon \partial J/\partial\epsilon|_{\epsilon_X}$  is the variance of the exchange noise. The approximate infidelity  $1 - P'_-$ , shown in the inset (right axis) of Fig. 2(a), shows good agreement with the numerical simulations using the full Hamiltonian.

In the solution (9), we kept the leading order contribution from exchange noise which goes as  $\sigma_J^2$ . This is a sufficient approximation at the optimal working point where  $g\mu_B B_z=0.75$   $\mu$ eV,  $\sigma_J \simeq (g\mu_B B_z/t_c)^2 \sigma_\epsilon \sim 7$  neV, which is of the order of the nuclear Zeeman energy for natural Si, and it can be further reduced by increasing  $t_c$ . Note that  $\sigma_J$  does not contribute to the dephasing time in (9), which is set by the nuclear noise variance of  $\Delta h_x$  (cf. Eq. (E7)), yielding  $T_2^*(X)=310$  ns, consistent with our numerical simulations of  $X$  rotations shown in Fig. 2(d). Instead, the leading effect of exchange noise is to cause small random misorientations of the rotation axis away from  $X$ .<sup>34</sup> From Eq. (9), this effect contributes to the infidelity as  $1 - P'_- \sim (\sigma_J/\Delta B_x)^2 \sim \sigma_\epsilon^2 B_z^4/t_c^4 \Delta B_x^2$ , leading to the  $B_z$  dependence to the right of the minimum that dominates the infidelity, as shown in the inset of Fig. 2(a). This scaling relation shows that increasing  $\Delta B_x$  cannot suppress detuning noise while keeping leakage fixed, which requires fixed  $B_z/\Delta B_x$ . On the other hand, reducing the ratio  $B_z/t_c$  while keeping leakage ( $B_z/\Delta B_x$ ) fixed can significantly reduce the detuning noise contribution to the infidelity.

### B. $Z$ rotations

We next consider the fidelity of pulsed  $Z$  rotations. After optimizing  $X$ -rotations with respect to applied magnetic fields, the detuning  $\epsilon_z$  can be still be tuned to opti-

mize  $Z$  gates. We note that the presence of  $\Delta B_x$  causes a rotation axis ( $Z'$ ) that is tilted away from  $Z$  in the  $X$ - $Z$  plane by angle  $\theta = \tan^{-1}[\Delta B_x / \sqrt{2}(B_z - J(\epsilon_{Z'}))]$ . If desired, a true  $Z$ -rotation can be implemented via a three-step pulse sequence, provided that  $\theta < 45^\circ$ .<sup>28</sup> A conventional Ramsey sequence containing three rotations,  $X_{\pi/2}$ - $Z_\pi$ - $X_{\pi/2}$  can be achieved with the multi-pulse sequence shown in Fig. 1(c). Here, we simulate just the  $Z'(\pi)$  portion of this sequence. Beginning with the initial state  $|X\rangle = (|S\rangle + |T_-\rangle) / \sqrt{2}$ , on the equator of the  $S$ - $T_-$  Bloch sphere, we suddenly pulse to  $\epsilon_{Z'}$  and evolve the system for a  $\pi$  rotation period. We then compute the rotation fidelity  $f(Z'_\pi) = P(-X) / V$ , where  $P(-X)$  is the probabilities of reaching the final state  $|-X\rangle$  and  $V = \cos^2 \theta$  is the visibility, defined as the maximum amplitude for an ideal  $Z'$  rotation.<sup>39</sup>

The results of our simulations are shown in Fig. 2(c). Here, we have used several nearly optimal magnetic field values for  $\Delta B_x$  and  $B_z$  obtained for  $X_\pi$  rotations. We find an optimal fidelity of about 99.5% at  $\epsilon_{Z'} \simeq -1.5$  meV, corresponding to a gate frequency of 124 MHz and a tilt angle of  $\theta = 19.5^\circ$ . Fig. 2(e) shows long-lived  $Z'$  oscillations with  $T_2^*(Z') \simeq 300$  ns at the optimal point. Similar to  $X_\pi$  rotations, the optimal value of  $\epsilon_{Z'}$  is determined by the competing contributions between detuning noise and leakage to the infidelity,  $1 - f(Z'_\pi)$ . Denoting the optimal value by  $\epsilon_{Z'}^*$ , detuning noise and leakage dominates the infidelity when  $\epsilon_{Z'} > \epsilon_{Z'}^*$  and  $\epsilon_{Z'} < \epsilon_{Z'}^*$ , respectively. The leakage oscillations can be seen explicitly in the exact analytic solution to the noise-averaged  $Z'$ -rotation in the asymptotic limit  $\epsilon \rightarrow -\infty$ , where  $J \rightarrow 0$ , derived in Appendix F. Thus, although the  $\epsilon \rightarrow -\infty$  limit is a detuning sweet spot, the optimal working point occurs at finite  $\epsilon_{Z'}$ . Finally, we find a very high process fidelity at the optimal point  $F(Z'_\pi) = 99.9\%$ .

## V. CONCLUSIONS AND OUTLOOK

In conclusion, we propose a singlet-triplet qubit in the  $S$ - $T_-$  subspace, for which all rotation frequencies are set by applied magnetic fields. By simulating a quasistatic noise model, we have shown that in the regime  $\Delta B_x < B_z \ll t_c$ , the qubit is well protected from detuning noise due to a wide sweet spot at the  $S$ - $T_-$  crossing. The optimal magnetic fields are significantly smaller than previous proposals,<sup>19,37</sup> easy to attain in the laboratory, and yield fidelities exceeding 99% for rotations around two nearly orthogonal axes.

The fidelities predicted here depend on the input parameters in the simulations, and they can potentially be enhanced in several ways. First, charge noise can be reduced by using special gate geometries.<sup>33</sup> Second, both leakage and the dephasing mechanisms considered here can be suppressed by increasing the tunnel coupling and then re-optimizing the magnetic fields. Third, the nuclear noise can be reduced through isotopic purification or nuclear polarization.<sup>8,9,40,41</sup> We estimate that the

dominant dephasing mechanism would switch from nuclear to detuning noise by using 99.5% isotopically purified <sup>28</sup>Si, corresponding to  $\sigma_h < 0.2$  neV, see Appendix E3. At this level of purification, for  $t_c = 60$   $\mu$ eV and  $g\mu_B(\Delta B_x, B_z) = (0.1, 0.9)$   $\mu$ eV, our model gives a  $X_\pi$  gate fidelity of  $F(X_\pi) = 99.9\%$ .

While the analysis here has focused on DC pulsed gates, AC resonant gates have some advantages.<sup>42</sup> In particular, they allow all qubit operations to be performed at the sweet spot  $\epsilon_X$ , similar to recent experiments performed at a charge qubit sweet spot<sup>43</sup> that show significant improvements over DC gating. Finally, we note that in materials with large hyperfine or spin-orbit interactions (e.g., GaAs or InGaAs), the role of  $\Delta B_x$  could be replaced by polarized nuclear spins or a large spin-orbit coupling.<sup>44</sup>

This work was supported in part by NSF (PHY-1104660), NSF (DMR-1206915), ARO (W911NF-12-0607), UW-Madison Bridge Funding (150 486700 4), and by the Intelligence Community Postdoctoral Research Fellowship Program. The views and conclusions contained in this document are those of the authors and should not be interpreted as necessarily representing the official policies or endorsements, either expressed or implied, of the U.S. Government.

## Appendix A: Detuning dependent tunnel coupling

Recent experiments<sup>13,32</sup> suggest that the exchange energy may depend exponentially on the detuning in the far-detuned regime. At the same time, a constant coupling is consistent with experimental measurements over a range of detunings near the  $\epsilon = 0$  charge transition.<sup>13</sup> To model the exchange energy consistent with these experiments, we also consider a tunnel coupling with exponential dependence on detuning,  $t_c(\epsilon) = t_0 \exp(\epsilon/\epsilon_0)$ . Fitting the data from Ref. [13] to the form  $J \approx t_c(\epsilon)^2 / |\epsilon|$ , valid in the weak tunneling limit ( $t_c \ll |\epsilon|$ ) appropriate for the parameters in Ref. [13], we find  $\epsilon_0 = 6$  meV.

In Fig. 3, we plot the energy levels as a function of detuning for (i) constant tunnel coupling  $t_c = 20$   $\mu$ eV (solid lines) and (ii) detuning dependent tunnel coupling  $t_c(\epsilon)$  (dashed lines) with  $t_0 = 20$   $\mu$ eV and  $\epsilon_0 = 1$  meV, at optimal magnetic fields (The  $S'$  energy level is outside the range of the plot). The exchange energy in case (ii) drops more steeply than case (i), approaching zero at smaller detunings. As a result, both working points  $\epsilon_X$  and  $\epsilon_{Z'}$  occur at smaller values compared to the constant- $t_c$  model.

Table I shows the optimal  $X_\pi$  process fidelities  $F(X_\pi)$  for case (ii) with  $t_0 = 20$   $\mu$ eV, and for several values of  $\epsilon_0$  at the corresponding optimal magnetic fields. At  $\epsilon_0 = 1$  meV, the fidelity is slightly lower than that of case (i) reported in the main text. At  $\epsilon_0 = 10$  meV, the fidelity exceeds 99%. At  $\epsilon_0 \simeq 100$  meV, we recover the fidelity  $F(X_\pi) = 99.3\%$  of case (i).

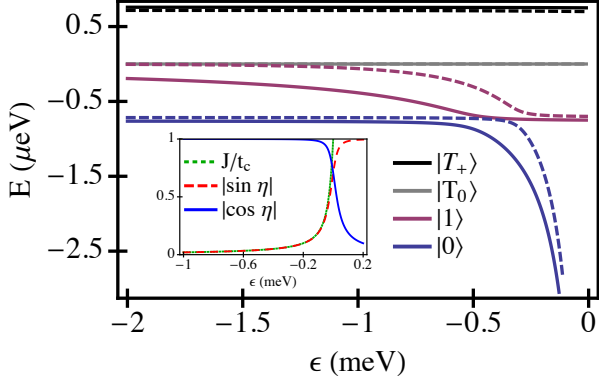


FIG. 3. (color online). Solid lines: The  $S-T_-$  qubit energy diagram including leakage states, as a function of detuning. The field parameters  $g\mu_B(\Delta B_x, B_z)=(0.25, 0.75)$   $\mu\text{eV}$  have been optimized for the constant tunnel coupling model with  $t_c=20$   $\mu\text{eV}$ , as described in the main text. On the right-hand side of the anticrossing, we have  $|0\rangle \simeq |S\rangle$  and  $|1\rangle \simeq |T_-\rangle$ . The high energy singlet  $|S'\rangle$  is separated by a large energy splitting and lies outside the range of this plot. Dashed lines: The corresponding energy diagram for the field parameters  $g\mu_B(\Delta B_x, B_z)=(0.3, 0.7)$   $\mu\text{eV}$ , which are optimized for the detuning-dependent tunnel coupling model with  $(t_0, \epsilon_0)=(20, 1100)$   $\mu\text{eV}$ . Inset: The magnitudes of the charge mixing angles ( $|\cos \eta|, |\sin \eta|$ ) and exchange energy  $J(\epsilon)$ .

$\epsilon_0$ (meV)	$g\mu_B \Delta B_x$ ( $\mu\text{eV}$ )	$g\mu_B B_z$ ( $\mu\text{eV}$ )	$F(X_\pi)$ (%)
1	0.3	0.7	98.5
10	0.25	0.75	99.2
100	0.25	0.75	99.3

TABLE I.  $X_\pi$  gate fidelities at optimal magnetic fields, for the detuning-dependent tunnel coupling model  $t_c(\epsilon)=t_0 e^{\epsilon/\epsilon_0}$ , with  $t_0=20$   $\mu\text{eV}$  and three different values of  $\epsilon_0$ .

## Appendix B: Effective $S-T_-$ Hamiltonian

In this section, we derive an effective  $2 \times 2$  Hamiltonian that includes corrections to Eq. (1) in the main text. These corrections are of order  $(\Delta B_\pm)^2/B_z$ , due to virtual transitions to  $T_0$  and  $T_+$  in second order perturbation theory.<sup>15</sup> As mentioned above,  $S'$  can be safely neglected in the  $(1, 1)$  regime, so we only need to consider the upper  $4 \times 4$  block of Eq. (2).

The effective Hamiltonian is defined as

$$H_{\text{eff}} = H^{(ST_-)} + \delta H^{(ST_-)},$$

where  $H^{(ST_-)}$  is the lowest order term in the  $2 \times 2$  Hamiltonian, as given in the main text, which is simply obtained by truncating terms outside the  $S-T_-$  manifold. The correction term is derived from nearly-degenerate perturbation theory as<sup>45</sup>

$$\delta H^{(ST_-)} = H_{PQ} \frac{1}{E - H_{QQ}} H_{QP}, \quad (\text{B1})$$

where  $H_{PP}=PHP=H^{(ST_-)}$ ,  $H_{QQ}=QHQ$ ,  $H_{QP}=QHP$ ,  $H_{PQ}=PHQ$ ,  $P=\sum_i |p_i\rangle\langle p_i|$  is the projection operator onto the  $S-T_-$  subspace with state labels  $p_i$ , and  $Q=\sum_i |q_i\rangle\langle q_i|$  is the projection operator onto the  $T_0-T_+$  subspace with state labels  $q_i$ . To leading order in the correction,  $E$  corresponds to the average energy eigenvalue of  $H^{(ST_-)}$ . At the  $S-T_-$  crossing, we have  $E=E_S=E_{T_-}=-B_z$ . Thus, the energy denominator is given by

$$\frac{1}{E - H_{QQ}} = \text{diag} \left( \frac{1}{E_S - E_{T_+}}, \frac{1}{E_S - E_{T_0}} \right) = -\text{diag} \left( \frac{1}{2B_z}, \frac{1}{B_z} \right),$$

neglecting corrections of order  $h_\pm/B_z$ . From Eq. (2), we have

$$H_{PQ} = \begin{pmatrix} \langle S|H|T_+ \rangle & \langle S|H|T_0 \rangle \\ \langle T_-|H|T_+ \rangle & \langle T_-|H|T_0 \rangle \end{pmatrix} = \begin{pmatrix} \cos \eta \frac{\Delta B_+}{2\sqrt{2}} & \cos \eta \frac{\Delta B_z}{2} \\ 0 & \frac{h_+}{2} \end{pmatrix},$$

and  $H_{PQ}=H_{QP}^\dagger$ . We then find that

$$\delta H_{ST} = -\frac{g\mu_B}{4B_z} \begin{pmatrix} \cos^2 \eta [(\Delta B_+ + \Delta h_+)(\Delta B_- + \Delta h_-)/4 + (\Delta B_z + \Delta h_z)^2] & \cos \eta h_- (\Delta B_z + \Delta h_z) \\ \cos \eta h_+ (\Delta B_z + \Delta h_z) & h_- h_+ \end{pmatrix}.$$

Thus, the leading order correction to  $H_{\text{eff}}$  is

$$\delta H_{ST}^{(0)} = -g\mu_B \cos^2 \eta \frac{\Delta B_+ \Delta B_- / 4 + \Delta B_z^2}{4B_z} \frac{1 + \tau_z}{2}. \quad (\text{B2})$$

This term slightly shifts the detuning location of  $X_-$



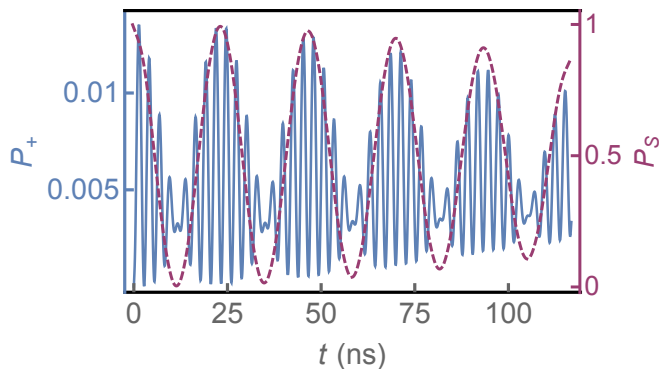


FIG. 4. (color online). Probability  $P_+$  of leaking into  $|T_+\rangle$  as a function of time  $t$  during  $X$ -rotations, for  $g\mu_B(\Delta B_x, B_z) = (0.25, 0.75) \mu\text{eV}$ . The envelope of the oscillations closely follows the probability  $P_S$  of  $|S\rangle$ , shown as the maroon, dashed line (right-hand axis).

rotations, whose position is defined by  $\text{Tr}[\tau_Z H_{\text{eff}}(\epsilon_X)] = 0$ , which now also depends on  $\Delta B_{\pm}$ . However, in the optimal operating regime of the  $S$ - $T_-$  qubit, we find that this correction is negligible.

### Appendix C: leakage

In this appendix, we consider transitions to the leakage states  $T_+$ ,  $T_0$ , and  $S'$ . From our numerical simulations, we find that the leakage probabilities for states  $T_0$  and  $S'$  are of the order  $P_0 \simeq 10^{-5}$  and  $P_{S'} \simeq 10^{-10}$ , respectively, which are negligible. The main leakage state is  $T_+$ , and its probability during  $X$ -rotations is plotted in Fig. 4 for  $g\mu_B(\Delta B_x, B_z) = (0.25, 0.75) \mu\text{eV}$ . The leakage exhibits oscillations with two frequencies: the characteristic frequency of the leakage state,  $2g\mu_B B_z/\hbar$ , and the  $X$ -rotations frequency,  $g\mu_B \Delta B_x/\sqrt{2}\hbar$ . The low frequency modulation is proportional to the singlet probability because  $T_-$  does not couple directly to  $T_+$ . We verify this by plotting the singlet probability  $P_S$  in Fig. 4 with dashed lines that clearly follow the envelope of the  $T_+$  oscillations. The leakage probability is consistent with the transition probability from  $S$  to  $T_+$  estimated with the Rabi formula, which agrees with perturbation theory for short times:<sup>46</sup>

$$P_+ \propto P_S \left( \frac{\Delta B_x/\sqrt{2}}{2B_z} \right)^2 \sin^2(g\mu_B B_z t/\hbar), \quad (\text{C1})$$

assuming an initial singlet probability of  $P_S$ . Note that in Fig. 4, the leakage oscillations goes through a local minimum of  $P_+ \simeq 0.003$  for  $X_{\pi}$  gate. This minimum is actually the maximum of the local minima in the leakage oscillations. As we mentioned in the main text, one can tune the magnetic fields to these leakage minima, where the rotation and leakage frequencies are commensurate.

Thus, even smaller leakage can be achieved for optimized gates with shorter periods, for example, the  $X_{\pi/2}$  gate.

We can estimate the leakage probability to  $T_0$  at the detuning  $\epsilon_X$  that would occur due to a finite  $\Delta B_z$  as a result of misalignment of the gradient field  $\Delta \mathbf{B}$  from being orthogonal to the quantization axis, by using Eq. (C1), making the replacement of the matrix element  $\Delta B_x/\sqrt{2} \rightarrow \Delta B_z$  and of the energy splitting  $2B_z \rightarrow B_z$ . The ratio of leakage to  $T_0$  and  $T_+$  is thus given by  $P_0/P_+ = 8(\Delta B_z/\Delta B_x)^2$ . Therefore, even for a large misalignment  $\Delta B_z/\Delta B_x \sim 10^{-1}$ , we have  $P_0 \simeq 8 \times 10^{-2} P_+$ . From Fig. 4, on average  $P_+ \sim 10^{-2}$  at the optimal working, so that  $P_0 < 10^{-3}$ , which is negligible small.

### Appendix D: Single qubit process matrix

For single qubit processes, an explicit expression for  $\chi$  is given by<sup>36</sup>

$$\chi = \Lambda \begin{pmatrix} \rho'_1 & \rho'_2 \\ \rho'_3 & \rho'_4 \end{pmatrix} \Lambda, \quad \Lambda = \frac{1}{2} \begin{pmatrix} I & \tau_X \\ \tau_X & -I \end{pmatrix}, \quad (\text{D1})$$

where  $\rho'_i = \mathcal{E}(\rho_i)$ ,  $\rho_i$  is the basis  $\{|n\rangle\langle m|\}$ ,  $n, m = 0, 1$ , which can be expressed in terms of physical input states  $|Z\rangle = |S\rangle$ ,  $|-Z\rangle = |T_-\rangle$ ,  $|X\rangle = (|S\rangle + |T_-\rangle)/\sqrt{2}$ , and  $|Y\rangle = (|S\rangle + i|T_-\rangle)/\sqrt{2}$  as

$$\begin{aligned} \rho'_1 &= \mathcal{E}(|-Z\rangle\langle -Z|) & (\text{D2}) \\ \rho'_4 &= \mathcal{E}(|Z\rangle\langle Z|) \\ \rho'_2 &= \mathcal{E}(|X\rangle\langle X|) - i\mathcal{E}(|Y\rangle\langle Y|) - (1-i)(\rho'_1 + \rho'_4)/2 \\ \rho'_3 &= \mathcal{E}(|X\rangle\langle X|) + i\mathcal{E}(|Y\rangle\langle Y|) - (1+i)(\rho'_1 + \rho'_4)/2 \end{aligned}$$

The real and imaginary parts of  $\chi$  matrix elements for the  $X_{\pi}$  and  $Z'_{\pi}$  gates are plotted in Fig. 5.

### Appendix E: Qubit dephasing in the $S$ - $T_-$ subspace

In this section, we analyze the dephasing due to quasi-static variations of nuclear fields and of the exchange coupling noise within the qubit subspace, focusing on the  $X$ -rotations.<sup>47</sup> The qubit Hamiltonian, up to an overall shift in the energy, is given by  $H^{(ST_-)} = (\mathbf{b} + \delta\mathbf{b}) \cdot \boldsymbol{\tau}/2$ , where

$$\mathbf{b}(\epsilon) = -g\mu_B \left[ \frac{\Delta B_x}{\sqrt{2}} \hat{\mathbf{x}} + \left( B_z - \frac{J(\epsilon)}{g\mu_B} \right) \hat{\mathbf{z}} \right] \quad (\text{E1})$$

is the effective field in the  $S$ - $T_-$  qubit subspace, and

$$\delta\mathbf{b} = -g\mu_B \left[ \left( h_z - \frac{\delta J}{g\mu_B} \right) \hat{\mathbf{z}} + \frac{\Delta h_x}{\sqrt{2}} \hat{\mathbf{x}} + \frac{\Delta h_y}{\sqrt{2}} \hat{\mathbf{y}} \right] \quad (\text{E2})$$

is the field due to the noise terms. Here, we keep only the leading term in the effective Hamiltonian, and take  $\cos\eta = 1$ , as is appropriate near the working points of this qubit. In Eq. (E2),  $\delta J = J(\epsilon + \delta\epsilon) - J(\epsilon) \simeq \delta\epsilon(\partial J/\partial\epsilon)$

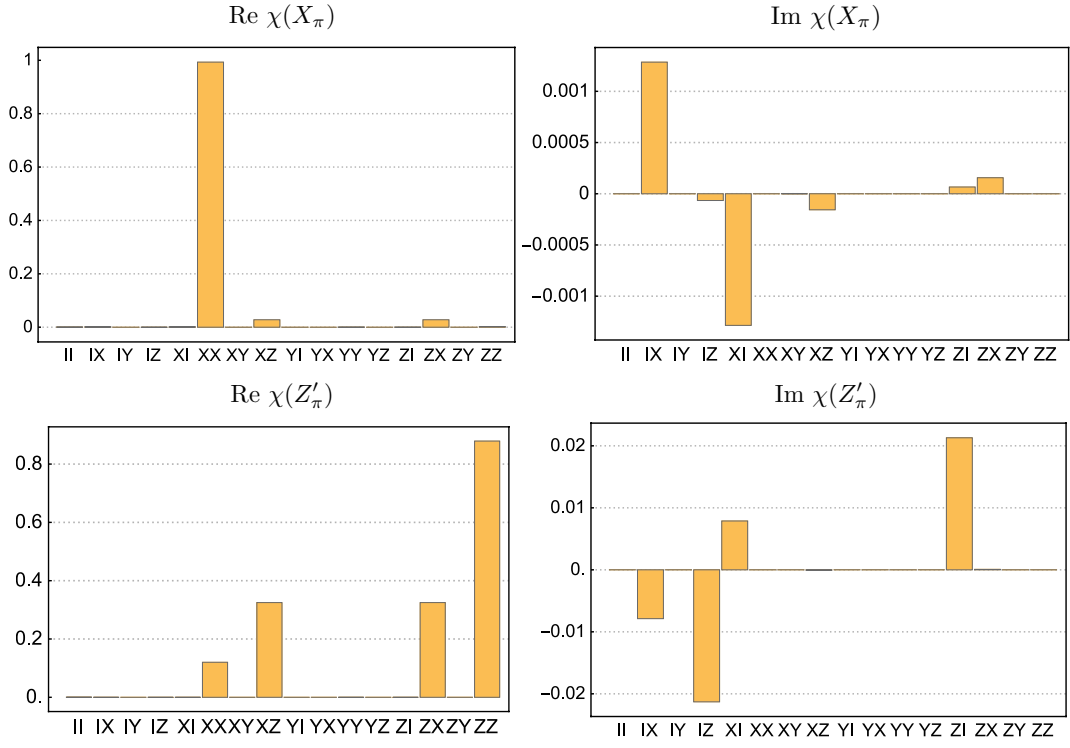


FIG. 5. The real and imaginary parts of the  $\chi$  matrix elements for  $X_\pi$  and  $Z'_\pi$  gates, computed with Eq. (D1).

is the fluctuation in the exchange energy arising from fluctuations of the detuning,  $\delta\epsilon$ , which is characterized by a the detuning-dependent variance given by  $\sigma_J = \sigma_\epsilon(\partial J/\partial\epsilon)$ . We denote by  $\hat{\tau}$  the Pauli matrices that span the  $S$ - $T_-$  subspace. (For example,  $\tau_Z = |S\rangle\langle S| - |T_-\rangle\langle T_-|$ .)

### 1. Pure dephasing rates

Here, we calculate the dephasing rate in the  $S$ - $T_-$  subspace. The energy splitting between the energy eigenstates  $|0\rangle$  and  $|1\rangle$  of the qubit Hamiltonian (4) is given by  $E_{01}=|\mathbf{b}|$ , and its fluctuation, up to quadratic order in the noise terms, is given by

$$\delta E_{01} \approx \delta b_{\parallel} + \frac{|\delta \mathbf{b}_{\perp}|^2}{2E_{01}}, \quad (\text{E3})$$

where  $\delta b_{\parallel} = \delta \mathbf{b} \cdot \hat{\mathbf{b}}$  and  $\delta \mathbf{b}_{\perp} = \delta \mathbf{b} - \delta b_{\parallel} \hat{\mathbf{b}}$  are the components of the noise field longitudinal and transverse to  $\hat{\mathbf{b}} = \mathbf{b}/|\mathbf{b}|$ , respectively. The expansion in Eq. (E3) requires  $\delta E_{01}/E_{01} \ll 1$ , which can potentially be violated by detuning noise since  $\sigma_\epsilon/g\mu_B \gg \Delta B_x, B_z$ , especially at the  $S$ - $T_-$  anticrossing  $\epsilon_X$ , where  $E_{01} = g\mu_B \Delta B_x/\sqrt{2}$  is at a minimum. However, as discussed below (9), in the optimal parameter regime (5),  $\sigma_h/\Delta B_x \sim \sigma_J/\Delta B_x \sim 10^{-2}$  at  $\epsilon_X$  and  $\epsilon_{Z'}$ , so that (E3) is valid for qubit rotations at the optimal working point.

The pure dephasing time scales are computed by averaging the relative dynamical phase factor between  $|0\rangle$  and  $|1\rangle$  with respect to the noise terms:

$$\overline{e^{i(\delta E_{01}t)/\hbar}} = \overline{e^{i\delta b_{\parallel}t/\hbar} e^{i\delta \mathbf{b}_{\perp}^2/2E_{01}}} \quad (\text{E4})$$

$$= e^{-(t/T_2^*(\epsilon))^2} W_{\perp}(t)$$

$$\overline{e^{i\delta b_{\parallel}t/\hbar}} \equiv e^{-(t/T_2^*(\epsilon))^2}, \quad (\text{E5})$$

$$\overline{e^{i\delta \mathbf{b}_{\perp}^2/2E_{01}}} \equiv W_{\perp}(t), \quad (\text{E6})$$

where the overbar denotes a noise average. For Gaussian distributions of  $\delta b_i$  with variances  $\sigma_i$ , the average of a generic function  $g(\delta \mathbf{b})$  is given by

$$\overline{g(\delta \mathbf{b})} = \prod_i \int \frac{d(\delta b_i)}{\sqrt{2\pi}\sigma_i} g(\delta \mathbf{b}) e^{-\delta b_i^2/2\sigma_i^2},$$

where  $\overline{\delta b_i} = 0$ ,  $\overline{\delta b_i \delta b_j} = \delta_{ij} \sigma_i^2$ , and  $i = x, y, z$ . Because the noise in orthogonal directions are uncorrelated, the longitudinal and transverse averages in Eq. (E4) can be separated. We first consider the leading, longitudinal contribution which gives rise to  $T_2^*(\epsilon)$ . The function  $W_{\perp}(t)$  is a decay envelope due to the subleading, transverse contribution that is only important (for optimal parameters) when the longitudinal nuclear noise is significantly reduced. (We will analyze this situation in Appendix E3, below.) Evaluating the average in Eq. (E5), one finds

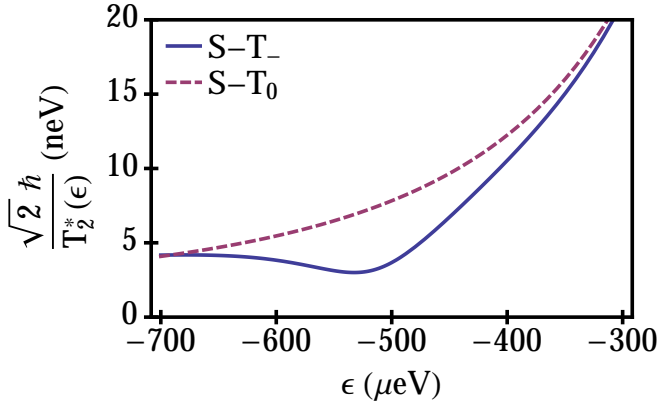


FIG. 6. A comparison of the dephasing rates for  $S-T_0$  and  $S-T_-$  qubits near the sweet spot  $\epsilon_X$ , for optimal magnetic fields of the  $S-T_-$  qubit, taking  $\Delta B_z = \Delta B_x/\sqrt{2}$  for the  $S-T_0$  qubit.

that

$$\begin{aligned} \frac{\sqrt{2}\hbar}{T_2^*(\epsilon)} &= \sqrt{\left(\sigma_J(\epsilon)\frac{\partial E_{01}}{\partial J}\right)^2 + \sigma_h^2 \left[ \left(\frac{\partial E_{01}}{\partial \Delta B_x}\right)^2 + \left(\frac{\partial E_{01}}{\partial B_z}\right)^2 \right]} \\ &= \sqrt{\frac{(\sigma_h^2 + \sigma_J(\epsilon)^2)(J(\epsilon)/g\mu_B - B_z)^2 + \sigma_h^2 \Delta B_x^2/2}{(J(\epsilon)/g\mu_B - B_z)^2 + \Delta B_x^2/2}}. \end{aligned} \quad (\text{E7})$$

At the sweet spot  $\epsilon_X$ , Eq. (E7) gives  $\sqrt{2}\hbar/T_2^*(\epsilon_X) = \sigma_h$ . We note that this is also a sweet spot for transverse fluctuations ( $h_z, \Delta h_y$ ) of the nuclear fields because  $\partial E_{01}/\partial B_z = 0$  and  $\partial E_{01}/\partial(\Delta B_y) = 0$  at  $\epsilon_X$ . For  $Z'$  rotations that occur in the far detuned regime where  $J \simeq 0$ , Eq. (E7) also predicts  $\sqrt{2}\hbar/T_2^*(\epsilon_{Z'}) \simeq \sigma_h$ . Physically, the nuclear noise sets the dephasing time for both rotation axes because both rotations are driven by magnetic fields, while the role of the detuning dependent exchange energy's is only to bring the  $S$  and  $T_-$  into resonance for the  $X$  rotations.

Finally, we note that the pure dephasing rate due to virtual occupation of the  $(0, 2)$  state,<sup>21,48</sup> given by  $\gamma \sin^2 \eta$ , where  $\gamma$  is the two-electron single dot dephasing rate, is strongly suppressed at the sweet spot. Taking  $\gamma \sim 10$  MHz<sup>49</sup> and noting that  $\sin \eta^2 \simeq (t_c/\epsilon_X)^2 \simeq (g\mu_B B_z/t_c)^2 = 10^{-3}$  at  $\epsilon_X$  (and smaller at  $\epsilon_{Z'}$ ), we find  $\gamma \sin^2 \eta \leq 10^{-2}$  MHz, which is negligible compared to the nuclear noise induced dephasing rate MHz.

## 2. Comparison with $S-T_0$ qubit

The key advantage of the  $S-T_-$  qubit is the presence of a detuning sweet spot  $\epsilon_X$  that protects  $X$ -rotations from exchange noise. It is instructive to compare these rotations with the exchange-driven rotations (“ $J$ ” gate)

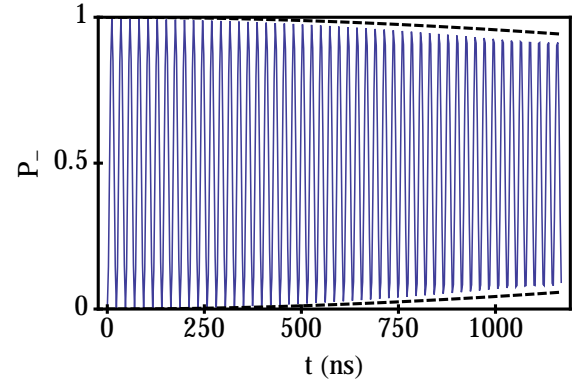


FIG. 7. The numerically computed probability  $P_-$  of occupying the  $T_-$  state as a function of time  $t$  during  $X$ -rotations in the absence of nuclear noise, for an initial singlet state  $S$ . The dephasing envelope (dashed lines) is given by Eq. (E10) with  $\sigma_h = 0$ .

of the  $S-T_0$  qubit, since for each qubit they correspond to the rotation axis that occurs at larger  $J$  and hence larger exchange noise  $\delta J$ . We next show that the dephasing time of the optimal  $S-T_-$  rotations are always longer than that of the  $S-T_0$  “ $J$ ” gate, for parameters such that the two qubits have the same rotation frequencies.

For  $S-T_0$  qubits, the effective field acting on the Bloch sphere is  $\mathbf{b} = J\hat{\mathbf{z}} + g\mu_B \Delta B_z \hat{\mathbf{x}}$ , which yields the following dephasing rate,<sup>32</sup>

$$\frac{\sqrt{2}\hbar}{T_2^{*(S-T_0)}} = \sqrt{\frac{(\sigma_J(\epsilon)J)^2 + 2(\sigma_h g\mu_B \Delta B_z)^2}{J^2 + (g\mu_B \Delta B_z)^2}}.$$

Since the  $S-T_0$  rotation frequencies for two near orthogonal axes are given by  $\hbar(\omega_1, \omega_2) = (g\mu_B \Delta B_z, \sqrt{J^2 + \Delta(g\mu_B \Delta B_z)^2})$ , we can set them equal to the  $S-T_-$  rotation frequencies by choosing  $J = g\mu_B B_z$  and  $\Delta B_z = B_x/\sqrt{2}$ . The  $S-T_0$  “ $J$ ” gate, with frequency  $\omega_2 = \omega_{Z'}$ , then occurs at  $\epsilon_X$ . We plot the dephasing rates for  $S-T_0$  and  $S-T_-$  qubits near the sweet spot  $\epsilon_X$  in Fig. 6, for optimal magnetic fields of the  $S-T_-$  qubit. In the figure, we see that the  $S-T_0$  dephasing rate at  $\epsilon_X \approx -500$   $\mu\text{eV}$  is about twice as fast as that of the  $S-T_-$  qubit.

## 3. Dephasing in the absence of nuclear noise

As described in Appendix E 1, the dephasing rate for  $X$ -rotations is set by the longitudinal nuclear noise. However, if nuclear noise is removed by isotopic purification or dynamic polarization, the detuning noise remains as a dephasing mechanism. As mentioned in Appendix E 1, detuning noise ( $\delta\epsilon$ ) at  $\epsilon_X$  is transverse to the  $X$  rotation axis and appears at quadratic order in the energy fluctuations, as given in Eq. (E3), yielding the decay envelope  $W_\perp(t)$  in Eq. (E6) which has a qualitatively different decay behavior than Eq. (E5). Here, we compare the

contribution to the dephasing rate for  $X$ -rotations due to transverse and longitudinal noise, and determine the nuclear noise variance that marks the crossover between nuclear vs. detuning noise-dominated dephasing.

The decay envelope  $W_{\perp}(t)$  at  $\epsilon_X$  is derived by averaging over the quadratic fluctuations. The Gaussian integral can be solved exactly:

$$W_{\perp}(t) = \overline{e^{i\delta\mathbf{b}_{\perp}^2 t/2\hbar E_{01}}} = \prod_{\alpha} \frac{1}{\sqrt{1 - i\sigma_{\alpha}^2 t/\hbar b}} \\ \approx e^{i\phi} e^{-(t/T_{2\perp}^*(X))^2}, \quad (\sigma_{\alpha}^2 t/2\hbar b \ll 1), \quad (\text{E8})$$

where the product is over the two transverse noise sources  $\sigma_J$  and  $\sigma_h$ ,  $\phi$  is an irrelevant phase that plays no role when we compute state probabilities,  $b=|\mathbf{b}(\epsilon_X)|=g\mu_B|\Delta B_x|/\sqrt{2}$  is the magnitude of the effective field of the Hamiltonian, and the transverse dephasing time is given by

$$T_{2\perp}^*(X) = \frac{2\hbar b}{\sigma_J^2 + \sigma_h^2}. \quad (\text{E9})$$

In the last line of Eq. (E8), we assume a short time limit, which is appropriate for the duration of a qubit gate ( $\tau_X \sim 1/b$ ), since  $\sigma_{\alpha}^2 \tau_X / \hbar b \sim \sigma_{\alpha}^2 / b^2 \ll 1$ . If we denote the longitudinal dephasing time obtained in the previous section as  $T_{2\parallel}^*(X) = \sqrt{2}\hbar/\sigma_h$ , then the combined, short-time decay function at  $\epsilon_X$  is given by  $\exp(-t^2/\tilde{T}_2^*(X)^2)$ , where

$$\frac{1}{\tilde{T}_2^*(X)^2} = \frac{1}{T_{2\perp}^*(X)^2} + \frac{1}{T_{2\parallel}^*(X)^2}. \quad (\text{E10})$$

Here, the shorter dephasing time naturally dominates the decay.

We now determine the crossover from nuclear to detuning noise-dominated decay, which can be implemented by isotopically purifying the sample with  $^{28}\text{Si}$ . The ratio of the longitudinal and transverse dephasing times is given by

$$\frac{T_{2\parallel}^*(X)}{T_{2\perp}^*(X)} = \frac{\sigma_J^2}{\sqrt{2}b\sigma_h} \left[ 1 + \left( \frac{\sigma_h}{\sigma_J} \right)^2 \right].$$

Solving for the crossover point which occurs when the ratio is equal to 1, we find  $\sigma_h \approx \sigma_J^2/\sqrt{2}b = 0.2$  neV. This happens when the abundance of  $^{29}\text{Si}$  is reduced from  $\sim 5\%$  (natural abundance) to  $\sim 0.5\%$ . At this level of purification, the total dephasing time is given by  $\tilde{T}_2^*(X) = 3.3$   $\mu\text{s}$ . In the limit of pure  $^{28}\text{Si}$ , we find the dephasing time  $T_{2\perp}^*(X) = 4.7$   $\mu\text{s}$ , which is due entirely to the remaining detuning noise. We demonstrate this limit in Fig. 7, which shows the numerically computed  $P_{-}$  probability for  $X$ -rotations. The dephasing envelope is predicted by Eq. (E10) with  $\sigma_h = 0$ . Note that we have not re-optimized with respect to magnetic fields here, which should give further improvements in the coherence time.

#### 4. Analytic solution in the $S$ - $T_{-}$ qubit subspace

In this appendix, we present the noise-averaged solution to the qubit equations of motion that follows governed by the 2D Hamiltonian (4). We apply the solution to the relaxation dynamics of a single electron spin in an external magnetic field with quasistatic fluctuations, derived in Ref. [34], to the pseudospin expectation value  $\mathbf{s} = \langle \psi | \boldsymbol{\tau} | \psi \rangle / 2$ , where  $|\psi\rangle = c_S |S\rangle + c_{-} |T_{-}\rangle$  is the state vector in the qubit subspace. As noted above, near the sweet spot  $\epsilon_X$ , all relevant noise sources have variance  $\sigma_{\alpha} \sim \text{neV}$ , so that  $\sigma_{\alpha}/\Delta B_x \sim 1\%$ . Therefore, we present this solution to the leading order in  $\sigma_{\alpha}/\Delta B_x$ .

Applying the results of Ref. [34] to  $X$ -rotations, for an initial state  $|S\rangle = |Z\rangle$ , we find the noise-averaged solution for pseudospin

$$\overline{\mathbf{s}(t)} = \frac{e^{-(t/T_2^*(X))^2}}{2} \left[ (\cos(\omega_X t) + 2\delta_{\perp}^2 \sin^2(\omega_X t/2)) \hat{\mathbf{z}} - \sin(\omega_X t) \hat{\mathbf{y}} \right], \quad (\text{E11})$$

where  $\omega_X = b/\hbar$ ,  $b = g\mu_B |\Delta B_x|/\sqrt{2}$ ,

$$\frac{\sqrt{2}\hbar}{T_2^*(X)} = \sigma_h, \quad \delta_{\perp}^2 = \frac{\sigma_J^2 + \sigma_h^2}{b^2}, \quad (\text{E12})$$

and  $\sigma_J = \sigma_{\epsilon}(\partial J/\partial \epsilon)|_{\epsilon_X}$ . As discussed in the previous appendix E1, the dephasing time is set by longitudinal noise from  $\Delta h_x$ . The exchange noise only gives a correction to the dephasing factor  $(\tau_X/T_2^*(X))^2$  that goes as  $(\sigma_J/\Delta B_x)^4$  [See Eq. (E9)], which is negligible compared to the contribution from  $\Delta h_x$  that goes as  $(\sigma_h/\Delta B_x)^2$ . (Corrections to the dephasing time due to the nuclear noise transverse to  $\Delta h_x$  are similarly suppressed.) The leading effect of the transverse noise is to cause fluctuations of the rotation axis, resulting in the term  $\sim \sin^2(\omega_X t/2)\delta_{\perp}^2$ . The final state probability ( $T_{-}$ ) for the  $X_{\pi}$  gate is given by  $P'_{-}(\tau_X) = 1/2 - \overline{s_z}(\tau_X)$ , where  $\tau_X = \pi/\omega_X$  is the gate time, which yields Eq. (9) in the main text.

#### Appendix F: Dephasing in the far-detuned regime

In this section, we present an analytic solution for  $Z'$  rotations in the asymptotic far-detuned regime for the full singlet-triplet subspace. This solution can be used to extract the nuclear noise variance  $\sigma_h$  from experimental data, and is valid for arbitrary values of the applied magnetic fields. Using this solution, we calculate a transition probability whose decay gives the coherence time between the  $S$  and  $T_{-}$  states. This is analogous to the nuclear noise induced decay of the singlet probability in the  $S$ - $T_0$  qubit calculated in Ref. [27], which gives the coherence time between the  $|\uparrow\downarrow\rangle$  and  $|\downarrow\uparrow\rangle$  states.

In the physically relevant  $4 \times 4$  subspace described in Appendix II, the Hamiltonian can be written in the

Heisenberg form

$$H = J(\epsilon) \left( \mathbf{S}_L \cdot \mathbf{S}_R - \frac{1}{4} \right) + g\mu_B \sum_{i=L,R} (\mathbf{B}_i + \mathbf{h}_i) \cdot \mathbf{S}_i. \quad (\text{F1})$$

In the far-detuned limit ( $\epsilon \rightarrow -\infty$ ), only (1,1) charge

states are occupied, and the exchange coupling  $J$  can be neglected. In this case, the system dynamics corresponds to individual spins precessing about their local magnetic fields, for which the time evolution operator (corresponding to  $Z'$  rotations) is given by

$$\begin{aligned} U(t) &= \exp(i\omega_L t \hat{\mathbf{n}}_L \cdot \boldsymbol{\sigma}_L) \otimes \exp(i\omega_R t \hat{\mathbf{n}}_R \cdot \boldsymbol{\sigma}_R) \\ &= \cos \omega_L t \cos \omega_R t + i \cos \omega_L t \sin \omega_R t \sum_{i=L,R} \hat{\mathbf{n}}_i \cdot \boldsymbol{\sigma}_i - \sin \omega_L t \sin \omega_R t (\hat{\mathbf{n}}_L \cdot \boldsymbol{\sigma}_L) \otimes (\hat{\mathbf{n}}_R \cdot \boldsymbol{\sigma}_R), \end{aligned}$$

where

$$\omega_i = \frac{g\mu_B |\mathbf{B}_i + \mathbf{h}_i|}{2\hbar} \quad \text{and} \quad \hat{\mathbf{n}}_i = \frac{\mathbf{B}_i + \mathbf{h}_i}{|\mathbf{B}_i + \mathbf{h}_i|}, \quad (i = L, R),$$

and  $\boldsymbol{\sigma}_L$  and  $\boldsymbol{\sigma}_R$  denote the spin operators on the left and right dots, respectively. Note that these operators differ from the  $\boldsymbol{\tau}$  operators previously defined for the logical qubits states.

Applying this solution to an initial state  $|X\rangle = (|S\rangle + |T_-\rangle)/\sqrt{2}$ , we calculate the probability  $P(-X) = |\langle -X|U(t)|X\rangle|^2$  of occupying  $|-X\rangle$  after a  $Z'$ -rotation. Here, the average is taken over all nuclear fields  $\mathbf{h}_{L,R}$ . The relevant amplitudes are readily computed:

$$\begin{aligned} \langle -X|U(t)|X\rangle &= \frac{1}{2} (\langle S|U|S\rangle - \langle T_-|U|T_-\rangle + 2i \text{Im}[\langle S|U|T_-\rangle]), \\ \langle S|U(t)|S\rangle &= \cos \omega_L t \cos \omega_R t + \sin \omega_L t \sin \omega_R t (\hat{\mathbf{n}}_L \cdot \hat{\mathbf{n}}_R), \\ \langle S|U(t)|T_-\rangle &= \frac{1}{\sqrt{2}} [\sin \omega_L t \sin \omega_R t (n_L^z n_R^+ - n_L^+ n_R^z) - i \cos \omega_L t \sin \omega_R t (n_L^+ - n_R^+)], \\ \langle T_-|U(t)|T_-\rangle &= \cos \omega_L t \cos \omega_R t - i \cos \omega_L t \sin \omega_R t (n_R^z + n_L^z) - \sin \omega_L t \sin \omega_R t (n_L^z n_R^z), \end{aligned} \quad (\text{F2})$$

where  $n_i^\pm = n_i^x \pm i n_i^y$  ( $i = L, R$ ).

We perform the nuclear average numerically, and the resulting probability  $P(-X)$  is plotted in Fig. 7 in time units of  $T_2^* = \sqrt{2}\hbar/\sigma_h$ . Here, we assume the optimal magnetic field values and  $\Delta B_z = 0$ . The results shown in Fig. 7 are obtained for  $J=0$ . It is interesting to compare them

with the analogous  $Z'$  oscillations, for  $J>0$ , which are plotted in Fig. 2(e) of the main text. The most striking feature of the  $J=0$  oscillations is the modulation due to leakage. This modulation is the reason that the second sweet spot, corresponding to  $\epsilon \rightarrow \infty$ , is not an optimal working point for  $Z'$ -rotations, as noted in the main text.

<sup>1</sup> F. A. Zwanenburg, A. S. Dzurak, A. Morello, M. Y. Simmons, L. C. L. Hollenberg, G. Klimeck, S. Rogge, S. N. Coppersmith, and M. A. Eriksson, *Rev. Mod. Phys.* **85**, 961 (2013).

<sup>2</sup> F. H. L. Koppens, C. Buizert, K. J. Tielrooij, I. T. Vink, K. C. Nowack, T. Meunier, L. P. Kouwenhoven, and L. M. K. Vandersypen, *Nature* **442**, 766 (2006).

<sup>3</sup> J. J. Pla, K. Y. Tan, J. P. Dehollain, W. H. Lim, J. J. L. Morton, D. N. Jamieson, A. S. Dzurak, and A. Morello, *Nature* **489**, 541 (2012).

<sup>4</sup> M. Veldhorst, J. Hwang, C. Yang, A. Leenstra, B. de Ronde, J. Dehollain, J. Muhonen, F. Hudson, K. Itoh, A. Morello, and A. Dzurak, "An addressable quantum dot qubit with fault-tolerant control fidelity,"

(2014), arXiv:1407.1950.

<sup>5</sup> M. Pioro-Ladrière, T. Obata, Y. Tokura, Y.-S. Shin, T. Kubo, K. Yoshida, T. Taniyama, and S. Tarucha, *Nat. Phys.* **4**, 776 (2008).

<sup>6</sup> K. C. Nowack, F. H. L. Koppens, Y. V. Nazarov, and L. M. K. Vandersypen, *Science* **318**, 1430 (2007).

<sup>7</sup> E. Kawakami, P. Scarlino, D. R. Ward, F. R. Braakman, D. E. Savage, M. G. Lagally, M. Friesen, S. N. Coppersmith, M. A. Eriksson, and L. M. K. Vandersypen, *Nature Nano.* **9**, 666 (2014).

<sup>8</sup> D. J. Reilly, J. M. Taylor, J. R. Petta, C. M. Marcus, M. P. Hanson, and A. C. Gossard, *Science* **321**, 817 (2008).

<sup>9</sup> S. Foletti, H. Bluhm, D. Mahalu, V. Umansky, and A. Yacoby, *Nature Physics* **5**, 903 (2009).

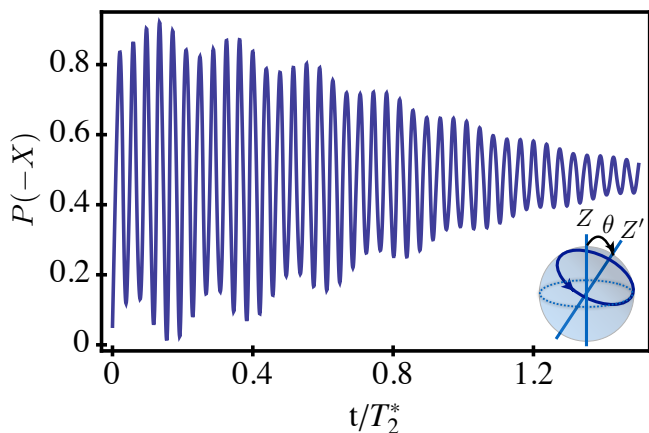


FIG. 8. The probability  $P(-X)$  of being in state  $|-X\rangle$  as a function of time  $t$ , for  $Z'$ -rotations around the equator of the Bloch sphere in the far-detuned regime where  $J(\epsilon) \approx 0$ . Solutions are obtained by numerically averaging the analytic solution given in Eq. (F2) over nuclear noise, for an initial state  $|X\rangle$  and optimal magnetic fields  $(\Delta B_x, B_z) = (0.25, 0.75) \mu eV$ .

<sup>10</sup> K. D. Petersson, L. W. McFaul, M. D. Schroer, M. Jung, J. M. Taylor, A. A. Houck, and J. R. Petta, *Nature* **490**, 380 (2012).

<sup>11</sup> J. R. Petta, A. C. Johnson, J. M. Taylor, E. A. Laird, A. Yacoby, M. D. Lukin, C. M. Marcus, M. P. Hanson, and A. C. Gossard, *Science* **309**, 2180 (2005).

<sup>12</sup> H. Bluhm, S. Foletti, I. Neder, M. Rudner, D. Mahalu, V. Umansky, and A. Yacoby, *Nature Physics* **7**, 109 (2011).

<sup>13</sup> B. M. Maune, M. G. Borselli, B. Huang, T. D. Ladd, P. W. Deelman, K. S. Holabird, A. A. Kiselev, I. Alvarado-Rodriguez, R. S. Ross, A. E. Schmitz, M. Sokolich, C. A. Watson, M. F. Gyure, and A. T. Hunter, *Nature* **481**, 344 (2012).

<sup>14</sup> X. Wu, D. R. Ward, J. R. Prance, D. Kim, J. K. Gamble, R. T. Mohr, Z. Shi, D. E. Savage, M. G. Lagally, M. Friesen, S. N. Coppersmith, and M. A. Eriksson, *Proceedings of the National Academy of Sciences* **111**, 11938 (2014).

<sup>15</sup> W. A. Coish and D. Loss, *Phys. Rev. B* **72**, 125337 (2005).

<sup>16</sup> W. A. Coish and D. Loss, *Phys. Rev. B* **75**, 161302 (2007).

<sup>17</sup> H. Ribeiro and G. Burkard, *Phys. Rev. Lett.* **102**, 216802 (2009).

<sup>18</sup> J. R. Petta, H. Lu, and A. C. Gossard, *Science* **327**, 669 (2010).

<sup>19</sup> H. Ribeiro, J. R. Petta, and G. Burkard, *Phys. Rev. B* **82**, 115445 (2010).

<sup>20</sup> L. Gaudreau, G. Granger, A. Kam, G. C. Aers, S. A. Studenikin, P. Zawadzki, M. Pioro-Ladrière, Z. R. Wasilewski, and A. S. Sachrajda, *Nature Physics* **8**, 54 (2012), arXiv:1106.3518 [cond-mat.mes-hall].

<sup>21</sup> H. Ribeiro, G. Burkard, J. R. Petta, H. Lu, and A. C. Gossard, *Phys. Rev. Lett.* **110**, 086804 (2013).

<sup>22</sup> S. A. Studenikin, G. C. Aers, G. Granger, L. Gaudreau, A. Kam, P. Zawadzki, Z. R. Wasilewski, and A. S. Sachrajda, *Phys. Rev. Lett.* **108**, 226802 (2012).

<sup>23</sup> A. G. Fowler, M. Mariantoni, J. M. Martinis, and A. N. Cleland, *Phys. Rev. A* **86**, 032324 (2012).

<sup>24</sup> An interdot Coulomb coupling can be included and ab-

sorbed into a redefinition of  $\epsilon$ .

<sup>25</sup> We assume the valley mixing energies are much larger than the tunnel coupling so that the excited valley states can be neglected.

<sup>26</sup> M. Prada, R. H. Blick, and R. Joynt, *Phys. Rev. B* **77**, 115438 (2008).

<sup>27</sup> J. M. Taylor, J. R. Petta, A. C. Johnson, A. Yacoby, C. M. Marcus, and M. D. Lukin, *Phys. Rev. B* **76**, 035315 (2007).

<sup>28</sup> R. Hanson and G. Burkard, *Phys. Rev. Lett.* **98**, 050502 (2007).

<sup>29</sup> L. V. C. Assali, H. M. Petrilli, R. B. Capaz, B. Koiller, X. Hu, and S. Das Sarma, *Phys. Rev. B* **83**, 165301 (2011).

<sup>30</sup> J. M. Taylor, H.-A. Engel, W. Dür, A. Yacoby, C. M. Marcus, P. Zoller, and M. D. Lukin, *Nature Physics* **1**, 177 (2005).

<sup>31</sup> M. D. Shulman, O. E. Dial, S. P. Harvey, H. Bluhm, V. Umansky, and A. Yacoby, *Science* **336**, 202 (2012).

<sup>32</sup> Dial, O. E. and Shulman, M. D. and Harvey, S. P. and Bluhm, H. and Umansky, V. and Yacoby, A., *Physical Review Letters* **110** (2013), 10.1103/PhysRevLett.110.146804.

<sup>33</sup> C. Buizert, F. H. L. Koppens, M. Pioro-Ladrière, H.-P. Tranitz, I. T. Vink, S. Tarucha, W. Wegscheider, and L. M. K. Vandersypen, *Phys. Rev. Lett.* **101**, 226603 (2008).

<sup>34</sup> I. A. Merkulov, A. L. Efros, and M. Rosen, *Phys. Rev. B* **65**, 205309 (2002).

<sup>35</sup> Z. Shi, C. B. Simmons, D. R. Ward, J. R. Prance, R. T. Mohr, T. S. Koh, J. K. Gamble, X. Wu, D. E. Savage, M. G. Lagally, M. Friesen, S. N. Coppersmith, and M. A. Eriksson, *Phys. Rev. B* **88**, 075416 (2013).

<sup>36</sup> M. A. Nielsen and I. L. Chuang, *Quantum Computation and Quantum Information* (Cambridge University Press, Cambridge, 2000).

<sup>37</sup> S. Chesi, Y.-D. Wang, J. Yoneda, T. Otsuka, S. Tarucha, and D. Loss, *ArXiv e-prints* (2014), arXiv:1405.7618 [cond-mat.mes-hall].

<sup>38</sup> It may be possible to utilize the leakage state  $T_+$  to form a qutrit, but this would require more control parameters than available in the present setup.

<sup>39</sup> We note that while a Z rotation at  $\epsilon > \epsilon_X$  is possible at a large enough detuning where  $J(\epsilon)/g\mu_B - B_z \gg \Delta B_x$ , it would be very susceptible to charge noise as the slope  $dJ/d\epsilon$  is large, as shown in Fig. 1.

<sup>40</sup> A. Brataas and E. I. Rashba, *Phys. Rev. B* **84**, 045301 (2011).

<sup>41</sup> J. R. Petta, J. M. Taylor, A. C. Johnson, A. Yacoby, M. D. Lukin, C. M. Marcus, M. P. Hanson, and A. C. Gossard, *Phys. Rev. Lett.* **100**, 067601 (2008).

<sup>42</sup> M. D. Shulman, S. P. Harvey, J. M. Nichol, S. D. Bartlett, A. C. Doherty, V. Umansky, and A. Yacoby, "Suppressing qubit dephasing using real-time hamiltonian estimation," (2014), arXiv:1405.0485.

<sup>43</sup> D. Kim, D. R. Ward, C. B. Simmons, J. King Gamble, R. Blume-Kohout, E. Nielsen, D. E. Savage, M. G. Lagally, M. Friesen, S. N. Coppersmith, and M. A. Eriksson, *ArXiv e-prints* (2014), arXiv:1407.7607 [cond-mat.mes-hall].

<sup>44</sup> M. S. Rudner, I. Neder, L. S. Levitov, and B. I. Halperin, *Phys. Rev. B* **82**, 041311 (2010).

<sup>45</sup> P. Löwdin, *The Journal of Chemical Physics* **19**, 1396 (1951).

<sup>46</sup> J. Sakurai, *Modern Quantum Mechanics* (Addison-Wesley, 1994).

<sup>47</sup> We note that  $T_1$  relaxation of the singlet-triplet states is

negligible, as singlet triplet life times have been measured to be ms at zero magnetic field and longer in applied fields Ref. [50].

<sup>48</sup> S. D. Barrett and C. H. W. Barnes, Phys. Rev. B **66**, 125318 (2002).

<sup>49</sup> J. K. Gamble, X. Hu, M. Friesen, and S. N. Coppersmith,

Phys. Rev. B **86**, 035302 (2012).

<sup>50</sup> J. R. Prance, Z. Shi, C. B. Simmons, D. E. Savage, M. G. Lagally, L. R. Schreiber, L. M. K. Vandersypen, M. Friesen, R. Joynt, S. N. Coppersmith, and M. A. Eriksson, Phys. Rev. Lett. **108**, 046808 (2012).